J Solid State Electrochem (2012) 16:3289–3297
DOI 10.1007/s10008-012-1769-5

ORIGINAL PAPER

Nanocomposite of polymerized ionic liquid and graphene used as modifier for direct electrochemistry of cytochrome c and nitric oxide biosensing

Huamao Chen · Guangchao Zhao

Received: 24 August 2011 / Revised: 29 April 2012 / Accepted: 2 May 2012 / Published online: 24 May 2012

Abstract In the present work, nanocomposite of polymerized ionic liquid (PIL), poly (1-vinyl-3-ethyl imidazolium) bromide, modified graphene nanosheet (PIL-Gr) was prepared. The PIL-Gr nanosheet composite was evaluated using scanning electron microscopy, transmission electron microscopy, and Fourier transform infrared spectroscopy. Then, a robust and effective sensing strategy based on the nanocomposite for cytochrome c (Cyt c) immobilization on basal plane graphite (BPG) electrode surface was proposed. Direct electrochemistry and electrocatalysis of immobilized Cyt c were investigated in detail. The cyclic voltammogram results indicated that the PIL-Gr nanocomposite film showed an obvious promotion for the direct electron transfer between Cyt c and the underlying electrode. The immobilized Cyt c exhibited an excellent electrocatalytic activity towards the reduction of nitric oxide (NO). The fabricated biosensor exhibited a fast response and a good electrochemical activity for NO with comparable liner range and low detection limit. The low apparent Michaelis–Menten constant (K_m^{app}) indicated the affinity of PIL-Gr and Cyt c. Moreover, the modified electrode displayed a rapid response to NO and possessed good stability and reproducibility. Based on the nanocomposite, a third-generation reagentless biosensor could be constructed for the determination of NO. The present work broadens the applications of graphene and ionic liquid in biosensor field.

Keywords Graphene · Polymerized ionic liquid · Nitric oxide · Cytochrome c · Biosensor

H. Chen · G. Zhao (✉)
Anhui Key Laboratory of Chem-Biosensing, School of Chemistry and Materials Science, Anhui Normal University, Wuhu 241000 Anhui, People's Republic of China
e-mail: gczhao@mail.ahnu.edu.cn

Introduction

Graphene, a new class of two-dimensional carbon nanostructure, has received an intense surge in interest because of its novel physical, chemical, and mechanical properties [1–3]. Owing to unique properties, graphene finds potential applications in many fields such as nanoelectronics, sensors, batteries, nanomaterials, supercapacitors, hydrogen storage, and resonators [4–6]. Recently, increasing attention has been paid on sensing fields in virtue of its excellent conductivity and electrocatalytic activity [7–9]. Various graphene-based electrochemical (bio)sensors have been developed to detect different kinds of analytes including important inorganic and organic electroactive molecules or compounds such as dopamine [10], β-nicotinamide adenine dinucleotide [11], guanosine [12], ethanol [13], glucose [13], nitrate [14], H_2O_2 [15], and NO [16, 17]. However, there are still many obstacles that limit the efforts of using graphene as electrochemical sensing materials, such as the poor understanding of electrochemical properties and aggregation of graphene in solution. To avoid aggregating, proper organic or inorganic solvent and stabilizing reagent were used, such as polymers (e.g., Nafion, sulfonated polyaniline, poly (methyl methacrylate), and polyacrylonitrile) [18–20], chitosan [16], ssDNA [21], and organic solvents such as *N*-methyl-2-pyrrolidone, *N*,*N*-dimethylformamide [22, 23], and ionic liquid (IL) [24–26].

Ionic liquid, comprising of large organic cations and various anions, is a novel type of non-aqueous but polar solvent. It has attracted a great deal of interest because of their unique chemical and physical properties such as negligible vapor pressure, high chemical and thermal stability, low toxicity, wide potential window, and high ionic conductivity [27]. In direct electrochemistry and electrocatalysis field, IL has been extensively used as materials for electrode

preparation and modification due to their properties of facilitating the direct electron transfer reaction between protein and electrode [28–30]. Recently, IL has been used as stabilizing reagent and/or binder reagent in constructing graphene-based sensors and biosensors [11, 25, 31]. However, ideal IL which could serve all the needs in establishing such kind of sensors and biosensors is scarcely obtained.

In the IL family, polymerized ionic liquid (PIL) is a group of functionalized ionic liquid which had been easily synthesized from the polymericable ionic liquid monomers [32, 33]. PIL possess not only the merits of IL but also the virtues of polymers, including good film stability, enhanced ionic conductivity, thermal stability, film forming ability, wide solubility, and high biocompatibility. This is quite helpful for the dispersion solution and stability of carbon-based material such as carbon nanotubes and graphene nanosheets [34, 35]. In addition, positively charged PIL and exchangeability of the counter-anions in PIL, e.g., with negatively charged proteins or enzymes in proper conditions, are much favorable for further immobilization of biomolecules [36]. Ruiz and co-workers developed a glucose amperometric biosensor based on the immobilization of glucose oxidase in microparticles prepared by polymerization of ionic liquid. The biosensor could be employed in aqueous and non-aqueous media for glucose determination in human serum samples [37]. In another paper, polymeric ionic liquid functionalized graphene was synthesized and immobilized onto glass carbon electrode to immobilize the negatively charged glucose oxidase through self-assembly for the detection of glucose [34]. However, there is still much work to do for synthesizing of PIL functionalized and also stabilized graphene nanocomposite and using in fabricating biosensors at the moment.

In our previous work, chitosan was used as protector and disperser to disperse graphene in aqueous solution. The as-prepared chitosan dispersed graphene was then immobilized on the surface of glassy carbon electrode to form a graphene modified electrode, and the direct electron transfer of Cyt c was achieved. The constructed Cyt c/graphene-based biosensor had displayed a potential application for nitric oxide biosensing [16]. To obtain a better graphene-based nanocomposite applying in biosensor, considering the proper quality of PIL as described previously, PIL was selected as protector and disperser for graphene-based nanocomposite preparation in this paper. First, we prepared poly (1-vinyl-3-ethyl imidazolium) bromide (PIL) functionalized graphene sheets (PIL-Gr) by a simple synthetic method, in which PIL could efficiently attach onto graphene to prevent the aggregation of graphene sheets through electrostatic repulsion. Subsequently, PIL-Gr was used as a modifier to modify the substrate electrode and immobilize Cyt c for construction of graphene-based electrochemical biosensor. PIL-Gr could provide a biocompatible microenvironment for the model protein and promote the electrotransfer between it and the underlying electrode. The fabricated biosensor exhibited a fast electron transfer of Cyt c and a good electrochemical activity for the detection of NO with wide liner range and low limit of detection. This indicated that the nanocomposite could be used as an excellent platform for realizing direct electrochemistry and electrocatalysis of redox proteins and establishing NO electrochemical biosensor.

Experimental

Materials

Cyt c was obtained from Sigma Chemical Company and used without further purification. Cyt c stock solution (5 mg mL^{-1}) was prepared by 0.1 M pH 7.0 PBS and stored at a temperature of 4 °C. The ionic liquid monomer 1-vinyl-3-ethyl imidazolium bromide ($ViEtIm^{+}Br^{-}$) was purchased from Shanghai Cheng Jie Chemical Co. Ltd. (ShangHai, China) and used as received. Graphene oxide (GO) was synthesized from graphite according to our previously reported paper [16]. Saturated NO solutions were self-made, and a fresh standard solution of NO was prepared daily for each experiment and kept in a glass vial sealed with a rubber septum. The NO concentration in the saturated solution was taken as 1.9 mM at 25 °C as reported. PBS (0.1 M) was prepared by mixing the stock solutions of Na_2HPO_4 and NaH_2PO_4 to proper pH. All other chemicals were of analytical grade and used as obtained. Double distilled water was used to prepare all solutions in the experiments.

Apparatus and procedure

All electrochemical experiments were performed on CHI 660B electrochemical workstation (CH Instruments, USA). A three-electrode system was used, where An Ag/AgCl electrode served as the reference electrode, a platinum wire electrode served as the auxiliary electrode, and a bare BPG electrode or modified BPG electrode was used as the working electrode. The surface morphologies of the prepared nanocomposite were observed through scanning electron microscopy (SEM) on S-4800 Scanning Electron Microscopy (Hitachi, Japan) at an accelerating voltage of 20 kV. Transmission electron microscopy (TEM) measurements were made on a Hitachi H-8100 electron microscope (Hitachi, Tokyo, Japan) operating at an accelerating voltage of 300 kV. The sample for TEM characterization was prepared by placing a drop of colloidal solution on carbon-coated copper grid and dried at room temperature. UV-visible spectra experiments were carried out on a UV-2540 UV–vis spectrophotometer (Shimadzu, Japan) with wavelength range of 350–500 nm. FT-IR spectra experiments

were obtained on an FTIR-8400S Fourier transform infrared spectroscopy (Shimadzu, Japan) with wavelength range of 500–3,800 cm^{-1}.

The electrochemical measurements were carried out in 10-mL cells containing 0.10-M PBS (pH 7.0) or 5.0-mM $[Fe(CN)_6]^{3-/4-}$ and 0.1-M KCl solutions. Prior to measurement, all electrolytic solutions were purged with high-purity nitrogen for at least 30 min, and then, a nitrogen atmosphere was maintained over the electrochemical cell during the experiments. The cyclic voltammograms (CVs) were recorded from −0.70 to 0.20 V or −1.0 to 0.10 V. All experiments were carried out at room temperature.

Synthesis of PIL-Gr nanosheets

PIL-Gr nanosheets were prepared as follow: (1) PIL was synthesized by a conventional free-radical polymerization. Inhibitors in the $ViEtIm^+Br^-$ monomer were removed by washing in diethyl ether in an iced bath, followed by drying under vacuum for 2 h in an iced bath. In a typical polymerization, imidazolium monomer $ViEtIm^+Br^-$ (5 g), 2, 2′-azobis(isobutyronitrile) (AIBN, 5 mg), and chloroform (30 mL) were charged to a 100 mL glass vial. The vial was sealed with silicon rubber-lined open-top cap and purged with N_2 via needles for 30 min and then immersed in an oil bath at 60 °C for 12 h. After polymerization, white-yellow solid precipitates appeared, and those were washed several times with chloroform. After drying under vacuum at 70 °C, 4.954 g of PIL was obtained (yield: 98 %). (2) GO was prepared according to our previously described literature [16]. The obtained brown dispersion was centrifuged for 30 min to remove any unexfoliated GO. The synthesized GO was dispersed in water to create a 0.8-mg mL^{-1} aqueous solution. (3) Preparation of aqueous dispersion of PIL-Gr nanosheets was the same with the procedures in the literature [35]. In details, 100 mg of PIL was mixed with 10 mL of the as-prepared GO dispersion (0.8 mg mL^{-1}), and the mixed solution was vigorously shaken for a few minutes. The resulting homogeneous dispersion was transferred into a 25-mL flask, followed by reduction with hydrazine monohydrate (10 mL) at 100 °C for 12 h. The color of the mixture solution changed from light yellow to black after the end of the reaction, indicating that graphene oxide had been reduced. Then, the mixture was centrifuged and washed with water three times. After redispersion, a stable black dispersion of PIL-Gr sheets in aqueous solution was obtained. The resulting PIL-Gr aqueous solution is stable for more than 2 months at ambient temperature.

Preparation of the Cyt c/PIL-Gr/BPG electrode

Prior to use, the BPG electrode was first polished with alumina slurry (followed by 1.0, 0.3, and 0.05 μm) on microcloth to mirror, cleaned with ethanol and double distilled water, and then dried in nitrogen. The effective area of the BPG electrode calculated from the cyclic voltammegrams of 5-mM $K_4[Fe(CN)_6]$ containing 0.1-M potassium chloride is 0.1624 cm^2. Then, 5 μL of the resulting PIL-Gr solution (about 0.03 %) was cast onto the clean BPG electrode surface, and the electrode was allowed to dry for 24 h to form a PIL-Gr modified electrode, noted as PIL-Gr/BPG electrode. Subsequently, the modified electrode was soaked in 2-mg mL^{-1} Cyt c solution (0.1-M PBS, pH 7.0) for 24 h at 4 °C so that Cyt c could be adsorbed on the modified electrode to create a Cyt c/PIL-Gr/BPG electrode. The Cyt c/PIL-Gr/BPG electrode was stored at 4 °C in a refrigerator when not in use. For comparison, Cyt c/BPG and Cyt c/PIL/BPG were prepared with the same procedures as described previously.

Results and discussion

Characterization of PIL-Gr nanosheets

PIL-Gr nanosheets, Gr together with GO, were first investigated by SEM, and Fig. 1 illustrated the typical results. As can be seen from Fig. 1a, b, the surface exhibits a curly morphology consisting of a thin wrinkling paper-like structure with nanometer size. In Fig. 1c, the PIL-Gr sheets were observed to form separated but a little thicker sheets with single structures. The morphology may suggest that PIL has been uniformly integrated with graphene.

The surface morphology of PIL-Gr nanosheets, Gr, and GO was further examined by TEM, and the images were depicted in Fig. 2. In Fig. 2a, GO flakes are nearly transparent, and some fold together. Large monolayer Gr nanosheets with slightly scrolled edges can be observed in Fig. 2b, and the resemblance of crumpled silk veil waves that were corrugated is intrinsic to graphene nanosheets [38]. Figure 2c shows that PIL-Gr nanosheets have almost the same characteristics with Gr. In this case, PIL layers coved the surface of the graphene nanosheets upon π–π stacking interaction to prevent the Gr nanosheets from aggregating and precipitating. While PIL could dissolve in solution easily, as a result, PIL-Gr nanosheets could be dispersed to individual sheet in solution and exhibit a very stable nature. The photographs of the insert in Fig. 2 also confirm that PIL-Gr (Fig. 2c) together with GO (Fig. 2a) was found to be stable and well dispersed in the aqueous phase without any agglomeration. Also, both the Go and PIL-Gr dispersions remained stable for months. In contrast, unfunctionalized Gr (Fig. 2b) cannot disperse properly in water. Precipitation of agglomerate nanosheets, which aggregated easily and suspended in solution, can be clearly observed. All of these indicate that the PIL could effectively serve as both stabilizing reagent and dispersant [34].

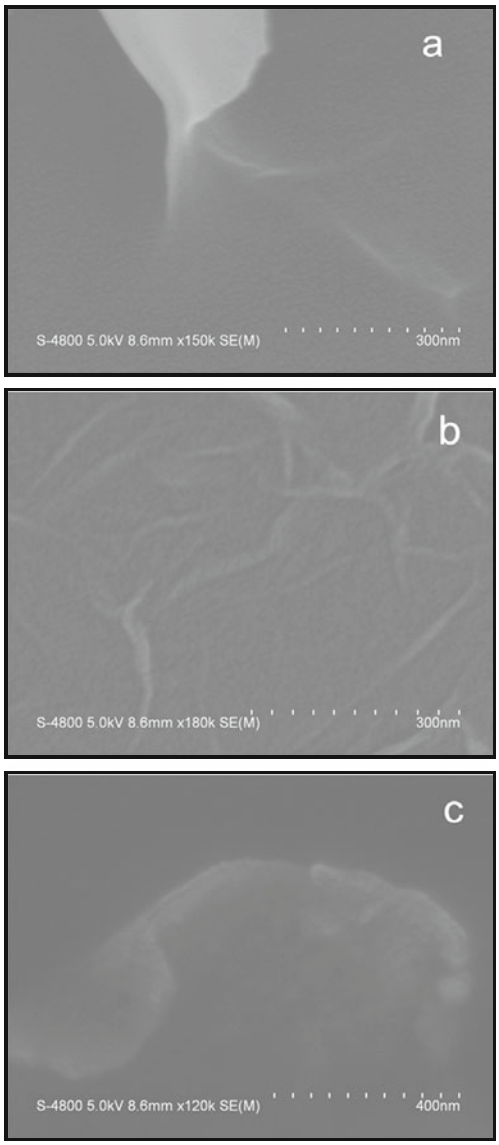

Fig. 1 SEM images of GO (**a**), Gr (**b**), and PIL-Gr nanosheets (**c**)

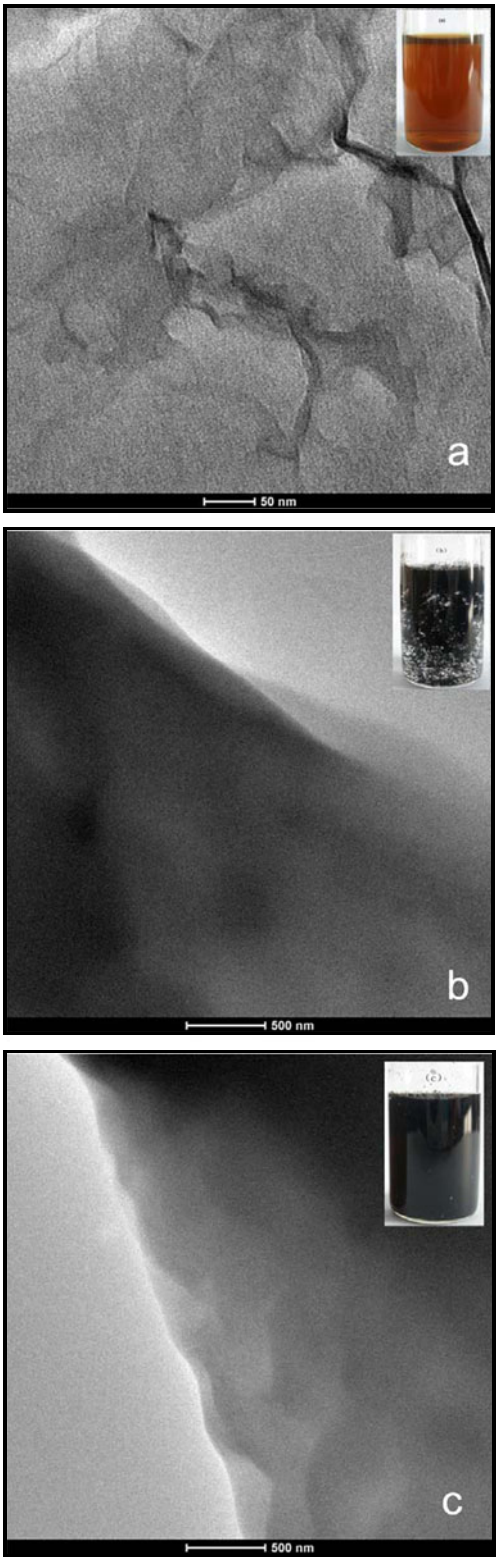

Fig. 2 TEM images of GO (**a**), Gr (**b**), and PIL-Gr nanosheets (**c**). *Inset* the photographs of the aqueous dispersion of GO (**a**), Gr (**b**), and PIL-Gr nanosheets (**c**)

FT-IR spectroscopy was also used to examine the PIL-Gr nanomaterials. PIL was confirmed in Fig. 3a, in which the presence of the C–H stretching bands located at 2,923 and 2,853 cm^{-1}, and the C–H vibration at 1,455 cm^{-1}, as well as the imidazolium framework vibration at 1,637 cm^{-1}, are evidenced. The spectrum of GO (Fig. 3b) shows the presence of O–H (ν_{O-H} at 3,365 cm^{-1}), C=O ($\nu_{C=O}$ at 1,667 cm^{-1} in carbonyl groups), C=C ($\nu_{C=C}$ at 1,445 cm^{-1}), and C–O (ν_{C-O} at 1,037 cm^{-1}). After the reduction, the disappearance of characteristic peaks of oxide groups in PIL-Gr (Fig. 3c) indicates that such graphene oxides have been fully reduced to the graphene. The FT-IR spectrum of PIL-Gr also exhibits PIL absorption features. The presence of the C–H stretching bands located at about 2,924 and 2,783 cm^{-1}, and the C–H vibration at 1,455 cm^{-1}, as well as the imidazolium framework vibration at 1,632 cm^{-1} are evidenced. Especially, the peak of the C–N stretch mode in PIL-Gr appears at 1,363 cm^{-1} (ν_{C-N} binding with aromatic

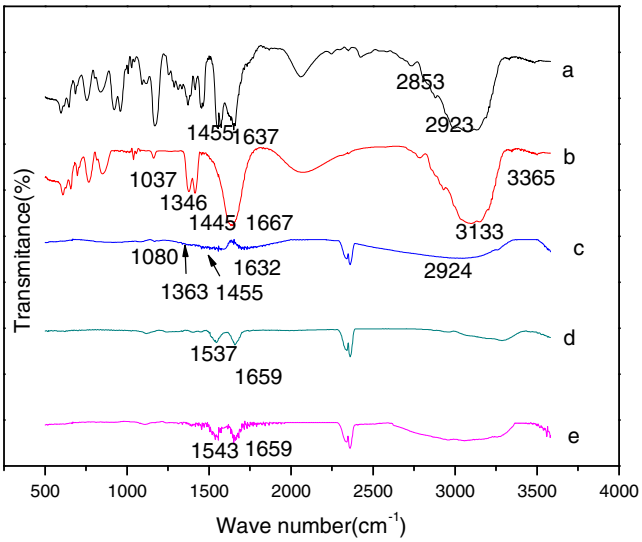

Fig. 3 FT-IR transmittance spectra of PIL (*a*), GO (*b*), PIL-Gr (*c*) , Cyt c (*d*), and Cyt c/ PIL-Gr (*e*)

ring). The shift might be attributed to the π–π stacking and hydrophobic forces between PIL and Gr. These results confirmed that the PIL has been covalently grafted to the graphene sheets successfully [18].

Potassium ferricyanide was selected as a probe to evaluate the electrochemical performance of the nanomaterials. Figure 4 shows the electrochemical responses of BPG, PIL/BPG, and PIL-Gr/BPG in 5-mM $K_4[Fe(CN)_6]$ and 0.1-M KCl solution, respectively. A pair of well-defined cyclic voltammograms with a peak-to-peak separation (ΔE_p) of 0.091 V was observed at the bare BPG electrode (Fig. 4a). After modified with PIL, the peak current increased obviously, and the ΔE_p decreased to 0.082 V (Fig. 4c), showing

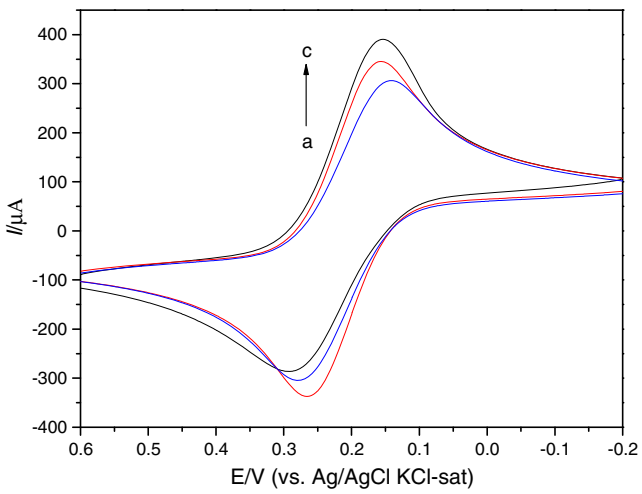

Fig. 4 Cyclic voltammograms of bare BPG (*a*), PIL-Gr/BPG (*b*), and PIL/BPG (*c*) electrodes in the presence of 5.0-mM $[Fe(CN)_6]^{3-/4-}$ containing 0.1-M KCl solution at a potential scan rat of 100 mV s^{-1}

that the PIL/BPG could accelerate the electron transfer of ferricyanide. This should ascribe to the good conductibility of PIL. While at the PIL-Gr/BPG (Fig. 4b), the peak current further increased, and the ΔE_p decreased a little (0.080 V). The smaller ΔE_p and larger peak currents of $[Fe(CN)_6]^{3-/4-}$ in Fig. 4b suggested that the PIL-Gr nanocomposite could further enhance the electron transfer rate of $[Fe(CN)_6]^{3-/4-}$. This was mainly due to the disappearance of negatively charged moieties present on graphene through chemical reduction and the increasement of conductivity of the graphene [39]. Further, the PIL was closely attached on the conductive graphene, synergistically enhanced the effective surface area of the electrode/electrolyte interfaces, and improved the charge transfer between the modifying layer and substrate BPG electrode. Although the increase of peak currents was partly due to the effect of preconcentration of hexacyanoferrates on PIL, the same surface charge characteristics of PIL and PIL-Gr probably resulted in the same preconcentration effect. Otherwise, the surface charge had no drastic effect on peak-to-peak separation [40]. Thus, the smaller ΔE_p and larger peak currents were on account of the introduction of PIL and Gr. Moreover, the attached protein/enzyme often had the similar negative charge as $[Fe(CN)_6]^{3-/4-}$ ions. As a result, the results indicate that PIL-Gr nanosheet film could effectively enhance the electrocatalytic activity and had a potential use in electroanalysis and electrochemical biosensor field.

Characteristics of Cyt c in PIL-Gr

FT-IR spectroscopy was used to detect the characteristic of Cyt c in PIL-Gr. Figure 3d, e shows the FT-IR spectrum of Cyt c and Cyt c/PIL-Gr, respectively. By comparison, amide I (1,659 cm^{-1}) and amide II (1,543 cm^{-1}) of Cyt c immobilized in PIL-Gr were nearly the same as those of native Cyt c. The slight shift of amide II band from 1,537 to 1,543 cm^{-1} might reveal the interaction between Cyt c and the PIL-Gr nanosheet film. Therefore, Cyt c entrapped in the PIL-Gr nanosheet film retained the essential features of native secondary structure, which accounted for that PIL-Gr that could provide a biocompatible microenvironment for Cyt c.

UV–vis spectroscopy is another effective means to probe the interaction between heme proteins and other materials. The wavelength and intensity of characteristic absorption spectra are sensitive to the conformational state of the protein [41]. Figure 5 shows the UV–vis spectra of PIL-Gr (Fig. 5a), Cyt c (Fig. 5b), and Cyt c/PIL-Gr composite films (Fig. 5c) on graphite slices. The Soret band of native Cyt c at 409 nm is the characteristic absorption band of oxidized state of Cyt c (ferricytochrome c). The Cyt c/PIL-Gr composite presented similar absorption bands as well, but the absorption band showed a red shift of 1 nm with the Soret band of 410 nm. The slight shift may well be ascribed to the

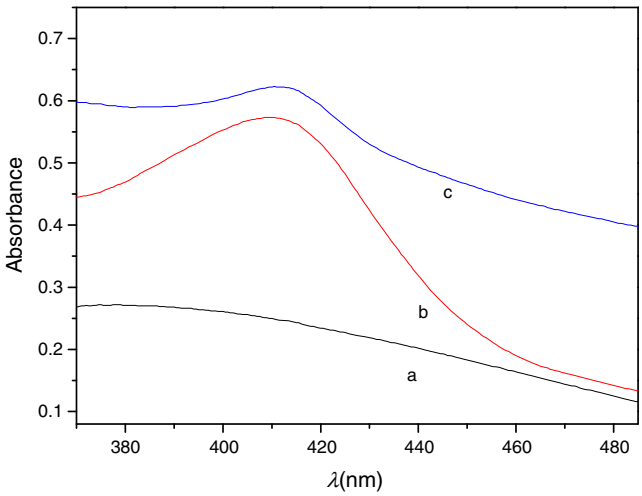

Fig. 5 UV–vis spectra of the PIL-Gr (*a*), Cyt c (*b*), and Cyt c/PIL-Gr films (*c*) on graphite slides

interaction between Cyt c and PIL-Gr, which indicates that Cyt c conformation remained nearly unchanged in PIL-Gr composite and that the PIL-Gr film might have good biocompatibility.

Voltammetric behaviors of the Cyt c/PIL-Gr/BPG electrode

The direct electrochemistry of Cyt c modified electrodes was studied by cyclic voltammetry. Figure 6 shows the CVs of different modified electrodes in 0.1-M PBS (pH 7.0) at a scan rate of 0.10 V s^{-1}. In the potential range from −0.7 to 0.2 V, no obvious redox peaks appeared at the Cyt c/BPG (Fig. 6a); this is possibly due to the unfavorable orientation or denaturing of Cyt c molecules on the bare BPG surface. At the PIL-Gr/BPG, there is also no redox peaks observed in the same potential range (Fig. 6b). While at the Cyt c/PIL/BPG, a couple of well-defined redox peaks was observed (Fig. 6c), corresponding to the direct electron transfer reaction between Cyt c and the underlying electrode. This demonstrated that the presence of PIL could facilitate the electron transfer between electrode and redox protein. However, a couple of stable, well-defined, and quasi-reversible waves appears at the Cyt c/PIL-Gr/BPG (Fig. 6d), together with the anodic peak potential (E_{pa}) of −0.211 V and the cathodic peak potential (E_{pc}) of −0.282 V, which means a quasi-reversible electrochemical process. Compared with Fig. 6c, in Fig. 6d, the peak-to-peak separation (ΔE_p) of 0.071 V and the formal potential $E^{\circ\prime}$ ($E^{\circ\prime}=(E_{pa}+E_{pc})/2$) of −0.247 V are similar. Nevertheless, the current responses of Cyt c are remarkably augmented, indicating that the PIL-Gr nanosheet film possessed larger surface area and further promoted the electron transfer rate of Cyt c. Thus, the interaction of PIL and Gr provided a remarkable synergistic promotion for the direct electrochemistry of Cyt c, which demonstrated the ability of the PIL to not only fortify the structure of Gr but also facilitate charge transport through the bulk of the nanosheet film, by providing less impeded pathways [42].

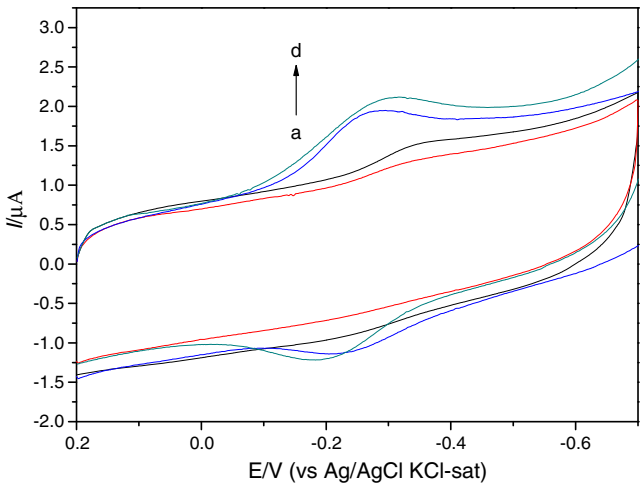

Fig. 6 CVs of Cyt c/BPG (*a*), PIL-Gr/BPG (*b*), Cyt c/PIL/BPG (*c*), and Cyt c/PIL-Gr/BPG electrodes (*d*) in 0.1-M PBS (pH 7.0) at a scan rate of 100 mV s^{-1}

We examined the CVs of Cyt c/PIL-Gr/BPG electrode in PBS (pH 7.0) at different scan rate. Both the anodic and cathodic peak currents increased with the increase of scan rate ν, and they are linearly proportional to ν in the wide range of 0.02–0.60 V s^{-1}. The linear regression equations for cathodic and anodic peaks were $I_{pc}=(3.62\pm0.02)\nu+(0.013\pm0.001)$ ($R=0.997$, I_{pc} in μA, ν in V s^{-1}) and $I_{pa}=-(3.54\pm0.01)\nu-(0.024\pm0.001)$ ($R=0.996$, I_{pa} in μA, ν in V s^{-1}), indicating a surface-confined electrochemical mechanism. With the increase of scan rate, the oxidation peak potential positively shifted, and the reduction peak potential negatively shifted, indicating that the redox reversibility of Cyt c was impaired. According to the equation $I_p = n^2F^2\nu A\Gamma^*/4RT$ [43], where ν is the scan rate, A is the modified electrode surface area, and the other symbols have their usual meanings. The surface concentration of electroactive Cyt c (Γ^*) at Cyt c/PIL-Gr/BPG was estimated to be 3.67×10^{-11} mol cm^{-2}, indicating that a monolayer of Cyt c participated in the electron-transfer process in the PIL-Gr nanosheet film. Under the surface controlled process, the electron transfer kinetics of Cyt c at the electrode can be obtained by using the approach developed by Laviron [43]. And the standard electron transfer rate constant (k_s) is expressed as the following equation:

$$\log k_s = \alpha\log(1-\alpha) + (1-\alpha)\log\alpha - \log\left(\frac{RT}{nF\nu}\right) - \frac{\alpha(1-\alpha)nF\Delta E_p}{2.3RT}$$

where α is the electron transfer coefficient, n is the electron transfer number, ν is the scan rate, and ΔE_p is the peak-to-peak separation. According to the equation, at the Cyt c/PIL-Gr/BPG, the value of k_s was calculated to be 2.39 s^{-1}. The k_s value is larger than that for Cyt c at graphene electrode (1.65 s^{-1}) [44] and Cyt c on colloidal Au (1.2 s^{-1}) [45], mesoporous SnO_2 film (1±0.03 s^{-1}) [46], GNPs/Chi/MWNTs (0.97 s^{-1}) [47], and poly-TTCA (5,2′:5,2″-terthiophene-3′-carboxylic acid) (1.86 s^{-1}) [48]. The faster k_s indicates that the PIL-Gr nanosheet film is an excellent promoter for the electron transfer between Cyt c and the underlying electrode.

The pH value of the supporting electrolyte also showed influence on the voltammetric behavior of Cyt c immobilized. We also surveyed the CVs of the Cyt c/PIL-Gr/BPG electrodes obtained in 0.1-M PBS (pH 7.0) at various pH values. The peak currents changed a little in the pH range of 4.0 to 9.0, which can be attributed to the changes of Cyt c activity and the promotion of PIL-Gr because they depend on pH to some extent. Furthermore, the formal potential shifted negatively along with the increase of pH value, and the relationship between the formal potential $E^{\circ\prime}$ and pH value was $E^{\circ\prime}=-0.056\text{pH}+0.071$ (R=0.998). The slope of 0.056 V pH^{-1}, which was close to the theoretical value (0.059 V pH^{-1}), implied a single-electron, single-proton transfer process.

Electrocatalysis of the Cyt c/PIL-Gr/BPG electrode

NO acts as a secondary messenger in signal pathways and an important regulatory molecule in the process of gene transcription and translation. As a result, there was a significant interest in developing new materials that can detect NO. Recently, many heme protein-based NO biosensors have been presented [49]. Nevertheless, constructing more sensitive, much rapid, and inexpensive NO biosensor with wider liner range and low detection limit is essential. Here, PIL-Gr had been proved to be a kind of superior material in modifying electrodes because of promoting the electrotransfer of Cyt c. Based on it, NO biosensor could be established. In order to explore the electrocatalytic activity of Cyt c on the PIL-Gr modified electrode, the response of the electrode to the reduction of NO was studied. Figure 7 is typical CVs of NO at the Cyt c/PIL-Gr/BPG electrode. With increasing concentration of NO, the reduction peak current of Cyt c increased obviously, while its oxidation peak current decreased to almost zero (Fig. 7b–e), showing a typical electrocatalytic reduction process of NO. However, no corresponding signal was visible at a Cyt c/BPG electrode under the same condition (Fig. 7a). This result illustrated that Cyt c in the PIL-Gr nanocomposite film retained its bioelectrocatalytic activity and exhibited excellent electrocatalytic activity towards

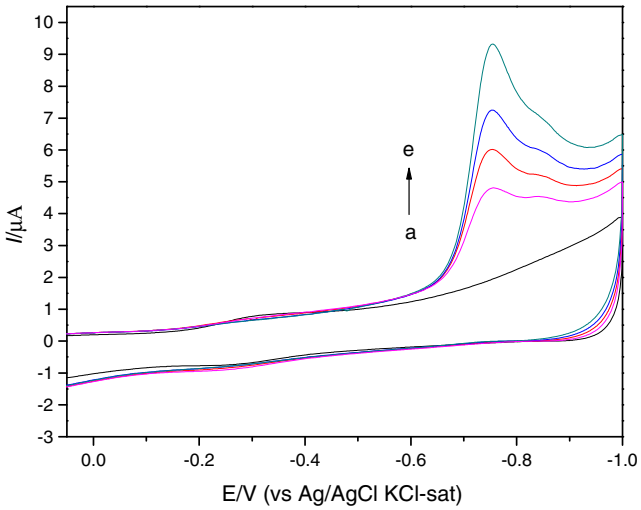

Fig. 7 CVs of bare BPG electrode (*a*) and the Cyt c/PIL-Gr/BPG electrode (*b–e*) at a scan rate of 100 mV s^{-1} in 0.1-M PBS (pH 7.0) with NO of different concentration (*a* 3.92, *b* 3.92, *c* 7.85, *d* 11.77, *e* 19.61 μM)

the reduction of NO. So, the Cyt c/PIL-Gr/BPG could be used as a NO biosensor.

Figure 8 illustrates a typical current–time plot for the Cyt c/PIL-Gr/BPG upon the successive addition of NO into stirring PBS (0.1 M, pH 7.0). Based on the optimal experiments, -0.73 V was selected as the applied potential for NO detection. The current response of the modified electrode increased along with NO concentration. The insert in Fig. 8 shows the calibration curve of current vs. concentration of NO. The modified electrode displayed increasing amperometric responses to NO with a linear range from 1.05×10^{-6} to 1.37×10^{-5} M (R=0.999, n=11), and the detection limit

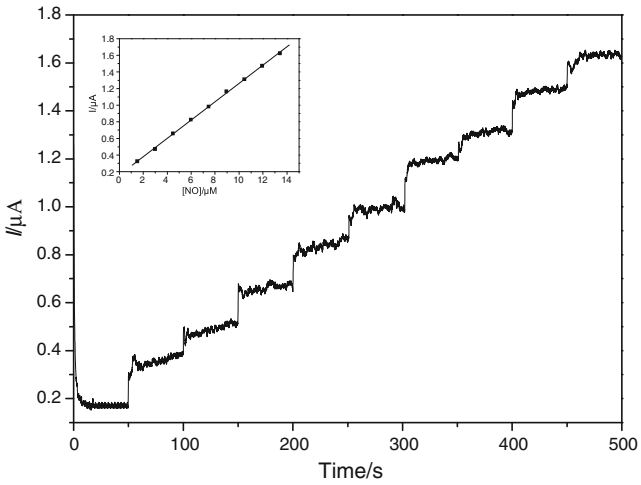

Fig. 8 Amperometric response of the biosensor to NO in PBS (pH 7.0) at an applied potential of −0.73 V upon successive additions of 1.05-μM NO. *Inset* plot of current vs. the concentration of NO

was 7.0×10^{-7} M at the signal-to-noise ratio of 3. Moreover, the electrode reached 95 % of the steady-state current within 3 s, suggesting that the response of the electrode to NO was a quick responsive process. The proposed Cyt c/PIL-Gr/BPG for NO determination was compared with other kinds of Cyt c modified electrode, and the results were illustrated in Table 1. It can be seen that this method can provide comparable linear range along with higher sensitivity and lower detection limit. When the concentration of NO further increased, a platform emerged in the cathodic peak current, showing the characteristics of Michaelis–Menten kinetics. The apparent Michaelis–Menten constant (K_m^{app}), which is an important parameter for enzyme-substrate reaction kinetics, can be estimated by the Lineweaver–Burk equation [50]:

$$\frac{1}{I_{ss}}=\frac{1}{I_{max}}+\frac{K_m^{app}}{I_{max}C}$$

where I_{ss} is the steady-state current after the addition of the substrate, I_{max} is the maximum current measured under saturated substrate conditions, and c is the bulk concentration of the substrate. Based on the experimental data from the inset of Fig. 8, the K_m^{app} value for the modified electrode was estimated to be 25.6 μM. This value was markedly smaller than 81.4 [51], 105.8 [52], and 320 μM [53], which implied that the Cyt c/PIL-Gr/BPG exhibited a quite higher affinity and activity to NO.

Selectivity, stability, and repeatability of the Cyt c/PIL-Gr/BPG

The selectivity of the NO biosensor was evaluated by NO determinations in the presence of some potentially coexisting compounds of NO in biological systems. These include ascorbic acid, uric acid, dopamine, catechol, and epinephrine. The detection of NO was not influenced by these potential interference compounds at concentrations 1–2 orders higher than expected in biological systems. Therefore, the NO biosensor has a good selectivity. The stability of the Cyt c/PIL-Gr/BPG electrode was studied as well. Even the 50 continuous cyclic scans were carried out in the potential range from −0.7 to 0.2 V with a scan rate of 100 mV s^{-1}; no obvious change of the CVs could be observed. Also, the relative standard deviation was 5.2 % for ten successive determinations of a 5-μM NO standard employing a single modified electrode. When the modified electrode was stored at 4 °C for about 2 weeks, the CV curve was still well retained, which suggested that the electrode had an excellent stability. The repeatability of the modified electrode was also investigated. In a series of five similarly prepared modified Cyt c/PIL-Gr/BPG electrodes, a relative standard deviation of 6.3 % was obtained for the individual current responses to the same sample, which revealed that the electrodes had an excellent repeatability.

Conclusions

A kind of more robust and advanced nanomaterial PIL-Gr was synthesized by introducing PIL to effectively improve the colligate properties of Gr. The PIL-Gr was modified on BPG electrode, and the direct electrochemistry of Cyt c in the nanosheet composite film was achieved. The integration of PIL and Gr provided a remarkable synergistic promotion for the direct electron transfer between Cyt c and the underlying electrode. The modified electrode showed an excellent electrocatalytic activity towards the reduction of NO along with low detection limit, quick response, good selectivity, stability, and repeatability. Based on the nanocomposite film, a third-generation reagentless biosensor could be constructed for the determination of NO. Comparing the chitosan dispersed graphene in our previous work, the PIL protected Gr was more stable in water together with comparable NO sensing ability. The PIL-Gr nanocomposite could also find a promising platform for other protein and enzyme immobilization together with biosensor preparation, and this work is worthy of promoting functionalized graphene-based electrochemical sensors and biosensor design.

Table 1 Comparisons of the responses of different Cyt c modified electrodes for NO determination

Electrode	Linear range (μM)	Detection limit (μM)	Sensitivity (μA μM^{-1})	Reference
Cyt c/SnO_2	1–13	1	–	[46]
Cyt c/poly-TTCA/Pt	2.4–55.0	0.13±0.003	0.117±0.006	[48]
Cyt c/DNA/GCE	0.6–8	0.1	–	[53]
Cyt c/MWNTs/GCE	2–48	1.3	–	[54]
Cyt c/CC/poly (5-NH_2-1-NAP)/GCE	0–34	2.85	0.15 (cm^{-2})	[55]
Cyt c/PIL-Gr/BPG	1.05–13.70	0.7	0.14	This work

SnO_2 mesoporous tin oxide film, *TTCA* 5,2′:5,2″-terthiophene-3′-carboxylic acid, *GCE* glass carbon electrode, *MWNTs* multi-walled nanotubes, *CC* cyanuric chloride, *poly (5-NH_2-1-NAP)* poly (5-amino-1-naphthol)

Acknowledgments This work was supported by the National Natural Science Foundation of China (20975001).

References

1. Meyer JC, Geim AK, Katsnelson MI, Novoselov KS, Booth TJ, Roth S (2007) Nature 446:60–63
2. Rao CNR, Sood AK, Subrahmanyam KS, Govindaraj A (2009) Angew Chem Int Ed 48:7752–7777
3. Bai H, Li C, Shi GQ (2011) Adv Mater 23:1089–1115
4. Schwierz F (2011) Nature 472:41–42
5. Jung JH, Jeon JH, Sridhar V, Oh IK (2011) Carbon 49:1279–1289
6. Chen D, Tang LH, Li JH (2010) Chem Soc Rev 39:3157–3180
7. Zhou K, Zhu Y, Yang X, Luo J, Li C, Luan S (2010) Electrochim Acta 55:3055–3060
8. Zhang Y, Sun X, Zhu L, Shen H, Jia N (2011) Electrochim Acta 56:1239–1245
9. Ratinac KR, Yang W, Gooding JJ, Thordarson P, Braet F (2011) Electroanalysis 23:803–826
10. Wang Y, Li YM, Tang LH, Lu J, Li JH (2009) Electrochem Commun 11:889–892
11. Shan C, Yang H, Han D, Zhang Q, Ivaska A, Niu L (2010) Biosens Bioelectron 25:1504–1508
12. Yin HS, Zhou YL, Ma Q, Ai SY, Chen QP, Zhu LS (2010) Talanta 82:1193–1199
13. Shan C, Yang H, Song J, Han D, Ivaska A, Niu L (2009) Anal Chem 81:2378–2382
14. Liu KP, Zhang JJ, Yang GH, Wang CM, Zhu JJ (2010) Electrochem Commun 12:402–405
15. Xu HF, Dai H, Chen GN (2010) Talanta 81:334–338
16. Wu JF, Xu MQ, Zhao GC (2010) Electrochem Commun 12:175–177
17. Ng SR, Guo CX, Li CM (2011) Electroanalysis 23:442–448
18. Choi BG, Park H, Park TJ, Yang MH, Kim JS, Jang SY, Heo NS, Lee SY, Kong J, Hong WH (2010) ACS Nano 4:2910–2918
19. Bai H, Xu Y, Zhao L, Li C, Shi G (2009) Chem Commun 13:1667–1669
20. Vadukumpully S, Paul J, Mahanta N, Valiyaveettil S (2011) Carbon 49:198–205
21. Patil AJ, Vickery JL, Scott TB, Mann S (2009) Adv Mater 21:3159–3164
22. Park S, An J, Jung I, Piner RD, An SJ, Li X, Velamakanni A, Ruoff RS (2009) Nano Lett 9:1593–1597
23. Liang Y, Wu D, Feng X, Mullen K (2009) Adv Mater 21:1679–1683
24. Liu N, Luo F, Wu H, Liu YH, Zhang C, Chen J (2008) Adv Funct Mater 18:1518–1525
25. Zhu C, Guo S, Zhai Y, Dong S (2010) Langmuir 26:7614–7618
26. Kim TY, Lee HW, Stoller M, Dreyer DR, Bielawski CW, Ruoff RS, Suh KS (2011) ACS Nano 5:436–442
27. Luo H, Dai S, Bonnesen P, Buchanan A, Holbrey J, Bridges N, Rogers R (2004) Anal Chem 76:3078–3083
28. Shiddiky MJA, Torriero AAJ (2011) Biosens Bioelectron 26:1775–1787
29. Zhao GC, Xu MQ, Ma J, Wei XW (2007) Electrochem Commun 9:920–924
30. Opallo M, Lesniewski A (2011) J Electroanal Chem 656:2–16
31. Yang MH, Choi BG, Park HS, Park TJ, Hong WH, Lee SY (2011) Electroanalysis 23:850–857
32. Kawano R, Katakabe T, Shimosawa H, Nazeeruddin MK, Grätzel M, Matsui H, Kitamura T, Tanabec N, Watanabe M (2010) Phys Chem Chem Phys 12:1916–1921
33. Buaki M, Aprile C, Dhakshinamoorthy A, Alvaro M, Garcia H (2009) Chem Eur J 15:13082–13089
34. Zhang Q, Wu S, Zhang L, Lu J, Verproot F, Liu Y, Xing Z, Li J, Song X-M (2011) Biosens Bioelectron 26:2632–2637
35. Zhou XS, Wu TB, Ding KL, Hu BJ, Hou MQ, Han BX (2010) Chem Commun 46:386–388
36. Gao RF, Zheng JB (2009) Electrochem Commun 11:608–611
37. López MS-P, Mecerreyes D, López-Cabarcos E, López-Ruiz B (2006) Biosens Bioelectron 21:2320–2328
38. Guo HL, Wang XF, Qian QY, Wang FB, Xia XH (2009) ACS Nano 3:2653–2659
39. Li D, Kaner RB (2008) Science 320:1170–1171
40. Alwarappan S, Erdem A, Liu C, Li CZ (2009) J Phys Chem C 113:8853–8857
41. Collinson M, Bowden EF (1992) Anal Chem 64:1470–1476
42. Saxena AP, Deepa M, Joshi AG, Bhandari S, Srivastava AK (2011) ACS Appl Mater Interfaces 3:1115–1126
43. Laviron E (1979) J Electroanal Chem 100:263–270
44. Alwarappan S, Joshi RK, Ram MK, Kumar A (2010) Appl Phys Lett 96:263702–263703
45. Zhang L, Jiang X, Niu L, Dong S (2006) Biosens Bioelectron 21:1107–1115
46. Topoglidis E, Astuti Y, Duriaux F, Grätzel M, Durrant JR (2003) Langmuir 19:6894–6900
47. Xiang C, Zou Y, Sun L, Xu F (2007) Talanta 74:206–211
48. Alvin Koh WC, Rahman MA, Choe ES, Lee DK, Shim Y-B (2008) Biosens Bioelectron 23:1374–1381
49. Hetrick EM, Schoenfisch MH (2009) Annu Rev Anal Chem 2:409–433
50. Kamin RA, Wilson GS (1980) Anal Chem 52:1198–1205
51. Pang J, Fan C, Liu X, Chen T, Li G (2003) Biosens Bioelectron 19:441–445
52. Xu Y, Hu C, Hu S (2010) Sensor Actuator B Chem 148:253–258
53. Liu YC, Zhao J, Wu WL, Yang ZS (2007) Electrochim Acta 52:4848–4852
54. Chen X, Long HY, Wu WL, Yang ZS (2009) Thin Solid Films 517:2787–2791
55. Takahashi SH, Torresi SIC (2009) Synth Met 159:2159–2161